Topology of active site geometries in HCP and FCC nanoparticles and surfaces

Constantinos D. Zeinalipour-Yazdi*

School of Health, Sport and Bioscience, University of East London, Stratford Campus, Water Lane, London E15 4LZ, UK

*Correspondence to: c.zeinalipour-yazdi@uel.ac.uk

Abstract

In this study the various local site topologies on metal NP and metal surfaces of HCP and FCC metals have been identified. The analysis with physical ball-and-stick molecular models demonstrates that the local site geometry can be fully described by *triangular* or *square* atom motifs that are either *bridge* or *atop* bound with additional labels that indicate whether the local site is on top of a *tetrahedral* or *octahedral* hole. Additionally, an angle between the structural motif surfaces is needed that shows the relative orientation between them. With this theoretical approach we find that there are 5 different b5-sites[1-3].

Keywords: HCP, FCC, active site, molecular models, topology, geometry, b5

Introduction

Taylor[4] recognised about a hundred years ago that catalytic surfaces may be defined by defect and steps in contrast to the Langmurian[5] view of catalysts, which supported the idea that the catalysis occurs by the catalyst flat surfaces. It is now established that heterogeneous catalysts can either perform the catalysis at surfaces or at steps, defects and adatoms among others.[6] Usually, the metal nanoparticle component in metal supported catalysts is not well defined as a function of particle size, geometry and nanoscopic structure. In addition to this, the local site of the catalyst is not a consistent atomic arrangement but in contrast can differ from one catalyst surface site to the other due to different arrangement of the metal atoms and additional support effects, such as charge transfer and polarisation effects.[7]

The decomposition of the structure of materials with geometric shapes has its origin about 2500 years ago from philosophical studies. The philosopher Plato thought that the elements fire, air, water and earth were composed of regular tetrahedra, octahedra, icosahedra and hexahedra (cubes), respectively. [8] Kepler used geometric shapes that had hexagonal symmetry to describe he structure of snowflakes in *De nive sexangula* (*On the Six-Cornered Snowflake*). [9]

There have been successful attempts to identify the surface topology and geometry on metal NP by means of coordination numbers.[10-12] There are both experimental and computational studies which identify the various adsorption sites of intermediates, the topology of the adsorption site (e.g. edge adsorption, adsorption at defects) and the energetics of the adsorption site (e.g. activation of molecules at sites that have a particular geometry) and such studies have been essential in the elucidation of reaction mechanisms.[6,13-18]

The experimental identification of local site geometries in catalysts remains a challenge. Some interesting studies in this regard have been reported, for example studies on zeolites have shown they can offer insight into structure-property relationships, which depend on the topology of the metal local sites. The topology of metal-oxygen binding sites in ZSM-5 has been explored via ^{17}O high-resolution Electron Paramagnetic Resonance (EPR) spectroscopy and it was found that only some sites are populated.[19] Sensitivity-enhanced nuclear-magnetic resonance (NMR) methods have been used to study the active sites in Zeolite doped with various metal such as ^{67}Zn, ^{71}Ga, and ^{119}Sn.[20] The influence of a Pt/silica catalyst topology and particle size has been studied for the hydrogenation of ethene where smaller NP

surface reaction inhibit the reaction kinetics.[21] 1.5 keV Na^+ low energy ion scattering revealed that bromine ions adsorb at the edges of Au nanoclusters supported on silicon dioxide surfaces due to positively charged edge atoms.[22] The adsorption of CO was studied with high-resolution synchrotron-based X-ray photoelectron spectroscopy (XPS) on Pd NPs supported on graphene and it was found to preferentially bind to bridge and 3-fold-hollow sites.[23] The strain at catalytic sites (i.e. interfaces, surfaces, defects) on Pt NPs was measured using high-precision scanning transmission electron microscopy (TEM) and it was found to affect the turnover frequency (TOF) of the catalyst.[24]

There are a few computational studies, which explore the effect of nanoparticle geometry and surface termination on the properties of the NP and on the adsorption and activation of reaction intermediates. Molecular dynamics (MD) simulations have been used to study the impact force between nanoparticles in vacuum and it was found that spherical nanoparticles are likely to enable some nonlinear dynamic phenomena.[25] The local particle morphology was found to be important in CO activation on iron NPs (0.5-1.4 nm) in which the activation energies varied by 0.9 eV depending on NP geometric size.[26] The various adsorption sites of molecular hydrogen on Co_3Mo_3N surfaces was studied in which dissociative chemisorption was shown to happen on Co_8 nanoclusters whereas molecular adsorption was found to occur on the molybdenum nitride framework.[6,27] A DFT study of the adsorption of H on doped gallium nanocluster hydrides, $Ga_{12}XH$ (X = B, C, Al, Si, P, Ga, Ge, and As) correlated the effect of frontier orbitals onto the regio-selectivity of H adsorption at the various sites of the cluster. [28] PdAu nanoclusters where studied for their adsorption of CO, NO and H_2 and it was found that atop adsorption is more favourable and relatively stronger on Pd than on Au. [29] The cluster size-dependent adsorption energy of CO on Pd NPs (Pd_n, n = 55−260) was found to be 15 kJ mol^{-1} lower than the extrapolated limit for 3-fold-hollow sites. [30] The intrinsic size- and coordination-dependent catalytic properties of Au NPs and nanoclusters (NC) with a particular structural motif had reactivity for catalytic CO oxidation. [31] An enhanced surface activity for the reverse water-gas shift reaction (WGSR) was found on Cu supported on ceria where the structure of the Cu-CuO site geometry was found to determine the catalytic activity. [32] GGA/PW91 calculations on bimetallic RuCu alloys show that core-shell structures based on the HCP core contain steps that are catalytically active for nitric oxide dissociation.[33]

It is therefore evident that the topology and local site geometry can be both studied via experimental methods such as high-resolution EPR, sensitivity enhanced NMR, high resolution XPS, high-resolution TEM and low energy ion scattering techniques as well as computational techniques such as DFT and MD. However, there is still much development needed in these approaches to unambiguously identify the various local geometric arrangements of catalytic sites. The exact catalytic site geometry in most of the above experimental and computational studies is not explicitly defined.

On the contrary, in this study ball-and-stick models are presented, of the various site geometries of HCP and FCC nanoparticles and surfaces with defects, in which the catalytic sites are explicitly defined via relationships from analytical geometry. Taking advantage of the property that the surface structure of a metal nanoparticle has some resemblance of the underlying structure, as these would maintain the metal-metal bonds at the lowest energy separation and at a geometry that is consistent with the coordination of surface atoms. This provides the opportunity of a variety of topological surface sites that a periodic crystal can have which could be due to steps, defects and ad-atoms. It is noted that the potential of surface reconstruction is not very drastic for metals and the surface structure is mainly the same apart from a weak contraction or even expansion of the lattice constant.[34] So it is valid to assume that the surface structure of a metal nanoparticle will have a large resemblance with the underlying periodic crystal, which could be either face-centered cubic (FCC) or hexagonal-close packed (HCP). In this study we analyse the various surface local site geometries for these two crystal structures using solutions from analytical geometry.

Results and Discussion

Nanoclusters are present in highly dispersed heterogeneous catalysts having different sizes and geometries. Their structure when very small can be studied using theoretical techniques, which include molecular mechanics (MM), molecular dynamics (MD) or density functional theory (DFT) calculations *i.e.,* by exploring the conformational space as a function of the total energy of the cluster geometry. Their structure can also be studied in special case by experimental methods in which, surface imaging techniques such as scanning tunneling microscopy (STM), atomic force microscopy (AFM), aberration-corrected tunneling electron microscopy (TEM)

are used to image the shape of nanocluster size particles on the surface of a catalyst and reveal which facets are exposed to the reactant feed-stream. Additionally, spectroscopic techniques have been used as indirect probes of the surface structure of catalysts such as high-resolution EPR, sensitivity enhanced NMR and high resolution XPS. Still further computational, experimental and theoretical studies are needed to address which the catalytic local site geometries are and how these affect the catalytic activity of catalyst under study.

The hexagonal-close packed (HCP) and face-centered cubic (FCC) structures have unit cells that can be composed of geometric shapes as the ones shown in Fig. 1. These are basically two geometric shapes, the *tehrahedral* and *octahedral*, which define the tetrahedral (T) and octahedral (O) holes in the ABAB and ABCA lattices. There is also half the octahedral shape, which is a *square pyramidal* structure and this appears at various surface terminations of the NP such as along the (100) planes which expose facets that have atoms arranged in squares. The *square* is a basic geometric shape that appears on surfaces of metals along with the equilateral triangle. Therefore, all the surfaces of NP and corrugated surfaces that are derived from the HCP and FCC crystal of solids are composed of repeating geometric shapes of equilateral squares and triangles. We find that using this theoretical approach, which uses analytical geometry to assess the various local site geometries of metal structure, is successful as it found the b5-site (equilateral-triangle-square with a common side), which was previously identified as the active site of a Ru catalysts.[1-3] It is therefore evident that the local geometric sites of catalysts can be described by analytical geometry as this is established in the following section.

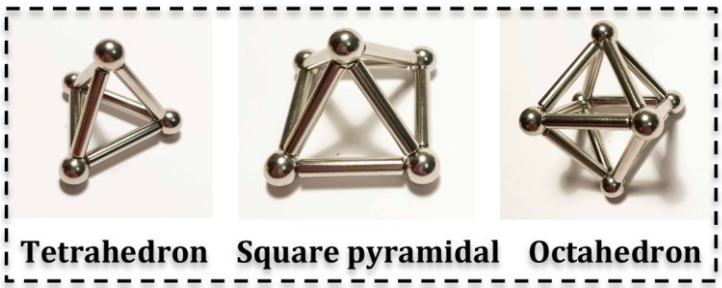

Fig. 1. Basic geometric shapes that can construct the FCC and HCP crystal

The topological geometry of local site geometry is described in this section. The various local site geometries are depicted in Fig. 2 and show that all local

geometric arrangements of active sites can be described with various combinations of equilateral squares and triangles that are either bond in bridge (b) or atop (t) conformation. The combination of two equilateral triangles results is 6 local site geometries three of which are atop bound and are 3f(T)-t-3f(T), 3f(O)-t-3f(T) and 3f(O)-t-3f(O), whereas the remaining are bridge bound, 3f(T)-b-3f(T), 3f(O)-b-3f(T) and 3f(O)-b-3f(O) (see Fig. 2). Furthermore, the combination of an equilateral square and triangle yields two local site structures, 3f(T)-b-4f and 3f(O)-b-4f whereas, the combination of two equilateral squares yields the local site, 4f-b-4f. Therefore, there is a total of 9 possible local site topologies, which can be further diversified by the introduction of an angle (which is shown by the yellow dashed line in Fig. 3) that describes the relative orientation between the two geometric motifs. Here it is noted that this convention has not been previously described elsewhere but certain sites such as the 3f-b-4f, has been previously labelled as the b5-site [2] which was found to be important in the ammonia synthesis [3] and decomposition [1] reaction over Ru surface steps. This b5-site exist at surface steps of HCP and FCC metals, as this can be seen in Fig. 3.

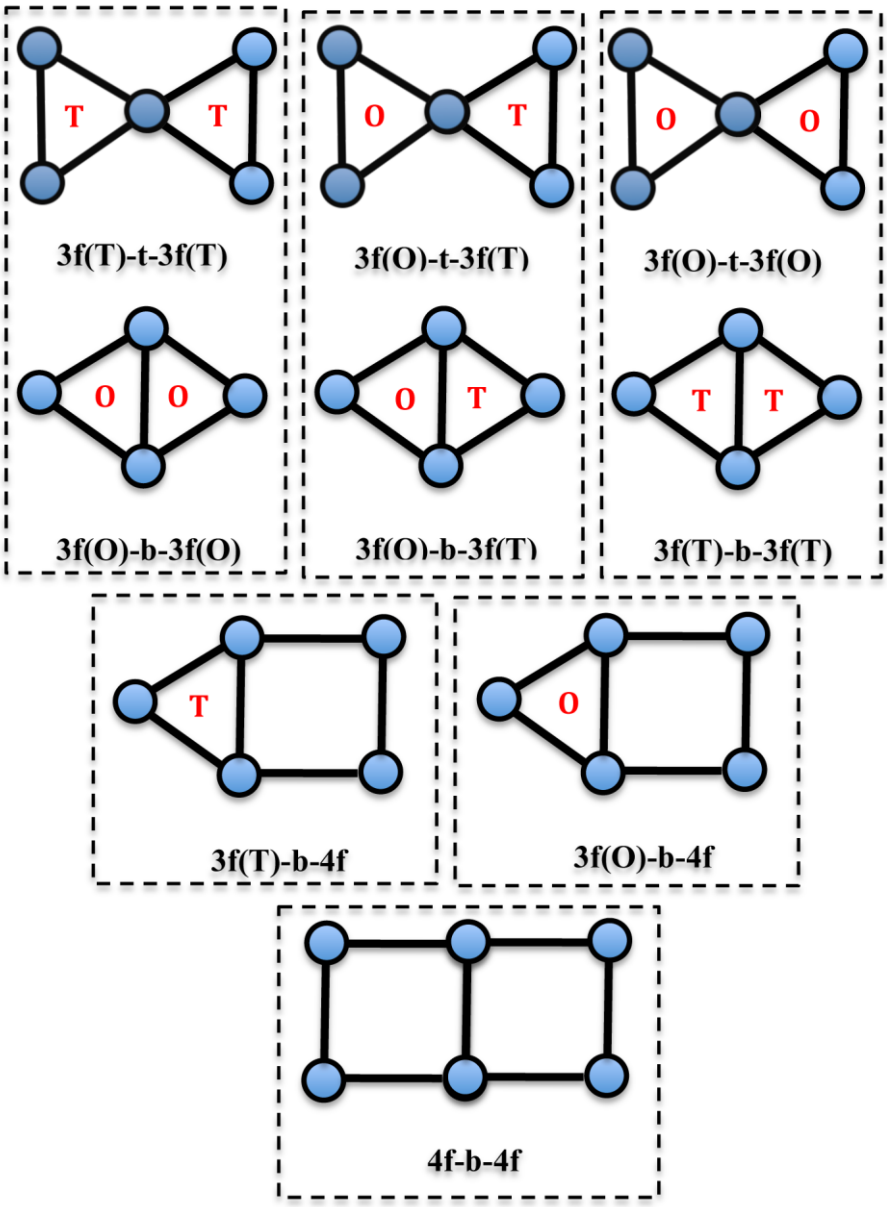

Fig. 2. Topology of different local site geometries on FCC and HCP nanoparticles. The dashed black line indicates the local site geometries that appear together on the nanoparticle

In Fig. 3 we show the various three-dimensional physical models of the various active sites using ball-and-stick models. These binding sites are made of the various three-dimensional geometric shapes depicted in Fig. 1 which are the basic geometric shapes of a tetrahedron, a square pyramid and an octahedron.

Local site 1, 3f(O)-b-3f(O)-250.5°, is made of just an octahedron and therefore the characteristic angle of the active site is 205.5°. The side view of this

octahedron resembles the general 3f(O)-b-3f(O), which means that there are two equilateral triangles bridge bound which are positioned directly above octahedral sites. This local site can be found at edges of HCP and FCC NPs and surfaces and binds adsorbates mostly at the bridge position. It can also bind larger molecules that have a curved structure and can simultaneously bind at the two three-fold hollow sites, that are in the center of the equilateral triangles. If a longer chain of such octahedrons is connected with intermediate tetrahedral angles so that the characteristic angle is maintained then an additional local site is found which has the general formula 3f(T)-t-3f(T) which has again a characteristic angle of 250.5°. Local site 1 seems to be a stable adsorption site in which the adsorbate is adsorbed through a bridged configuration. The characteristic angle is 250.5° therefore there is a high degree of unsaturation of the metal coordination, which suggests strong adsorption.

Local site 2, with the structure that resembles a b5-site has a general formula of a 3f(T)-b-4f site and is composed of a tetrahedron and a square pyramid in which the two triangular facets are connected. This local site has a characteristic angle of 234.7° and therefore receives the notation of 3f(T)-b-4f-234.7°. This local site can be found in both HCP and FCC NPs and is located above a tetrahedral hole. Local site 2 seems to be a stable adsorption site in which the adsorbate would adsorb to the four-fold hollow and the adjacent trigonal arrangement of the metal atoms. The chracteristic angle is 234.7° which suggests strong adsorption.

Local site 3 that is made of two octahedron bound each through one of their triangular facets has the general notation of 3f(O)-b-3f(O)-141.1° and is a relatively strong adsorption site for diatomic adsorbates such as CO, NO and $N_{2[27]}$ in which the multiple-bond is activated over the bridging site of this active site. It is the only local site that is located above two octahedral holes. Local site 3 is a very stable adsorption site and has a high degree of saturation of the metal atom coordination which suggests weaker adsorption of adsorbates.

Local site 4 can be found on the surface of both HCP and FCC crystals and corresponds to the (111) surface of these crystal packings. It is composed of tetrahedrons and octahedron placed in a two-dimensional array forming a completely flat arrangement of the metal atoms. Depending on whether the site is above tetrahedral sites or octahedral sites, this local site has two specific active sites with the notation of 3f(O)-b-3f(T)-180° and 3f(O)-t-3f(T)-180°, respectively. Local site 4 has a

moderate degree of saturation of the metal atom coordination and would resemble the adsorption at 111 surfaces of HCP and FCC metal surfaces

Local site 5 can be found both in linear arrays of HCP and FCC crystal edges. This local site is composed of two square pyramids and a tetrahedron bound in a complimentary arrangement so that flat surfaces form that have a repeating motif of square-square or square-triangular motifs. This arrangement of geometric shapes generates four different local site geometries some of which can be found on both HCP and FCC crystals. This local site has the characteristic angle of 180 deg. and therefore is given the notation of 4f-b-4f-180°. Local site 5 has a moderate degree of saturation of the metal atom coordination which suggests moderate adsorption of adsorbates. This adsorption will be similar to the adsorption to 100 surfaces of metals.

Local site 6, **local site 7** and **local site 8** which are the other three sites have higher characteristic angles and are given by the following notations, 3f(T)-b-3f(T)-289.5°, 3f(O)-t-3f(O)-289.5° and 4f-b-3f-305.27°, respectively. Local site 6, 7 and 8 have a high characteristic angle which suggests a highly unstable adsorption site which will result in strong adsorption of adsorbates

Local site 9 is made of an octahedron and a square pyramid which are bound through the triangular facets. This local site resembles again the b5-site and has a characteristic angle of 200.7° and therefore receives the notation of 4f-b-3f(O)-200.7°. This local site can be found on both HCP and FCC sites of NPs and is located above one octahedral hole. Local site 9 has a characteristic angle of 200.7° which implies that the catalytic site has moderate stability and therefore adsorption strengths will be moderate.

Local site 10 is another geometry that is made of an octahedron and a square pyramid, which are bonded via a bridge site. This geometry forms again a b5-site, which has a characteristic angle of 125.3° and is located above an octahedral hole. This local site geometric arrangement has the notation of 3f(O)-b-4f-125.3° and can be found on only HCP NPs and surface edges. Local site 10 has a small characteristic angle which suggests a very stable adsorption site which would result in a relatively weak adsorption of adsorbates.

Local site 11 is composed of three geometric shapes, two tetrahedrons and a square pyramid which form an angle of 109.5°. This active site that can be found on both HCP and FCC NP at sites which have adatoms and has the general notation of 4f(T)-b-3f(O)-109.5°. This local site is above an octahedral and above a tetrahedral

hole. Local site 11 has a characteristic angle of 109.5° which indicates a very stable metal atom configuration and should thus result in weak adsorption of adsorbates.

Local site 12 which is made of two square pyramids that are bound through their triangular facets. This active site is one of the few that has two adjacent square motifs at a characteristic of 250.5°. This local geometric site arrangement is found both in FCC and HCP NPs and has the notation of 4f-b-4f-250.5°. Local site 12 has a characteristic angle of 250.5° which means that the degree of metal atom saturation is low, suggesting a strong adsorption of adsorbates.

Local site 13 is made of a square pyramid and two tetrahedrons that are bound through their triangular facets. This local site arrangement again resembles the b5-site and is comprised of an equilateral square and a triangle bound through a bridge site, the triangle being above a tetrahedral hole. This local site can be found in both HCP and FCC NPs and has the general notation of 3f(T)-b-4f-164.2°. Local site 13 is one which has a b5-type configuration of the metal atoms. It is a moderately stable adsorption site with adsorption strengths of adsorbate that are moderate.

Local site 14 is composed of two square pyramids and a tetrahedron all bound through their triangular facets. This local site is again a b5-like site and can bind efficiently diatomics. It is found in both HCP and FCC crystals and has a general notation of 3f(T)-b-4f-125.3° as it is above one tetrahedral hole. Local site 14 has a b5-like configuration of the metal atoms. It is a very stable adsorption site with weak adsorption of the adsorbates.

Local site 15 which is made of two tetrahedron and one octahedron bound through their triangular facets can be found only in HCP NPs. It has a characteristic angle identical with that of a tetrahedron and receives the general notation of 3f(T)-b-3f(T)-109.5° as it is above two tetrahedral holes. Local site 15 is a very stable adsorption site with a very weak adsorption strength for diatomic adsorbates.

Local site 16 has a geometry that is composed of two tetrahedrons bound through their triangular facets. It is present in both HCP and FCC NP and has a characteristic angle of 219.0°. It therefore acquires the general notation of 3f(T)-b-3f(T)-219.0° as it is above two tetrahedral holes. Local site 16 has a characteristic angle of 219.0° which implies a moderate unsaturated electronic structure of the metal atoms and therefore moderate-to-strong adsorption of adsorbates.

Local site 17 is made of a square pyramid and an octahedron bound through their triangular facets. It can be found in both HCP and FCC crystals and has a

characteristic angle of 195.8°. It can bind diatomics well and has the general notation of 3f(O)-b-4f-195.8° as it is above one octahedral hole. Local site 17 has a characteristic angle of 195.8° which suggests a moderately stable adsorption site with only moderate adsorption strengths of adsorbates.

Local site 18 is a less common site and it is made of geometric shapes of two tetrahedron bound symmetrically through a C_{2v} axis through an atop site. This active site is found in both HCP and FCC NPs and has a characteristic angle of 240.0°. It therefore has the general notation of 3f(T)-t-3f(T)-240.0° and is located above two tetrahedral holes. Local site 18 has a very high characteristic angle which suggests a high uncoordinated nature of an atop metal atom. This results in isntability of the adsorption site and strong top-on adsorption of adsorbates.

It is noted that the characteristic angles shown by the yellow dashed line in Fig. 3 have been calculated by analytical geometry and are therefore angles that correspond to the perfect HCP and FCC like structures. These angles maybe slightly different if there is surface reconstruction or even surface lattice expansion/contraction. Nevertheless, they provide a mathematical recipe to uniquely define all the different active sites in HCP and FCC catalyst NPs and surfaces. Therefore the 18 local site geometric arrangements that can be used to label different active sites on metal nanoparticles and surfaces that have HCP and FCC crystals. These are most of the transition metals that are located in the d-block of the periodic table. We find that one local site, the b5-site that has been previously found on Ru catalyst could have different versions (i.e. **local site 2**, **local site 9**, **local site 10**, **local site 13** and **local site 14**) depending on the characteristic angle and whether the three-fold hollow is above an octahedral or a tetrahedral hole. As many as 18 local site geometries are found in HCP and FCC structures which can be uniquely defined according to the combination of square and triangular motifs, their binding (i.e. bridge or atop) and their characteristic angle. It is anticipated that this common method of classifying the local site geometries in catalyst may lead to a common convention in the labelling of active sites in metal catalysts.

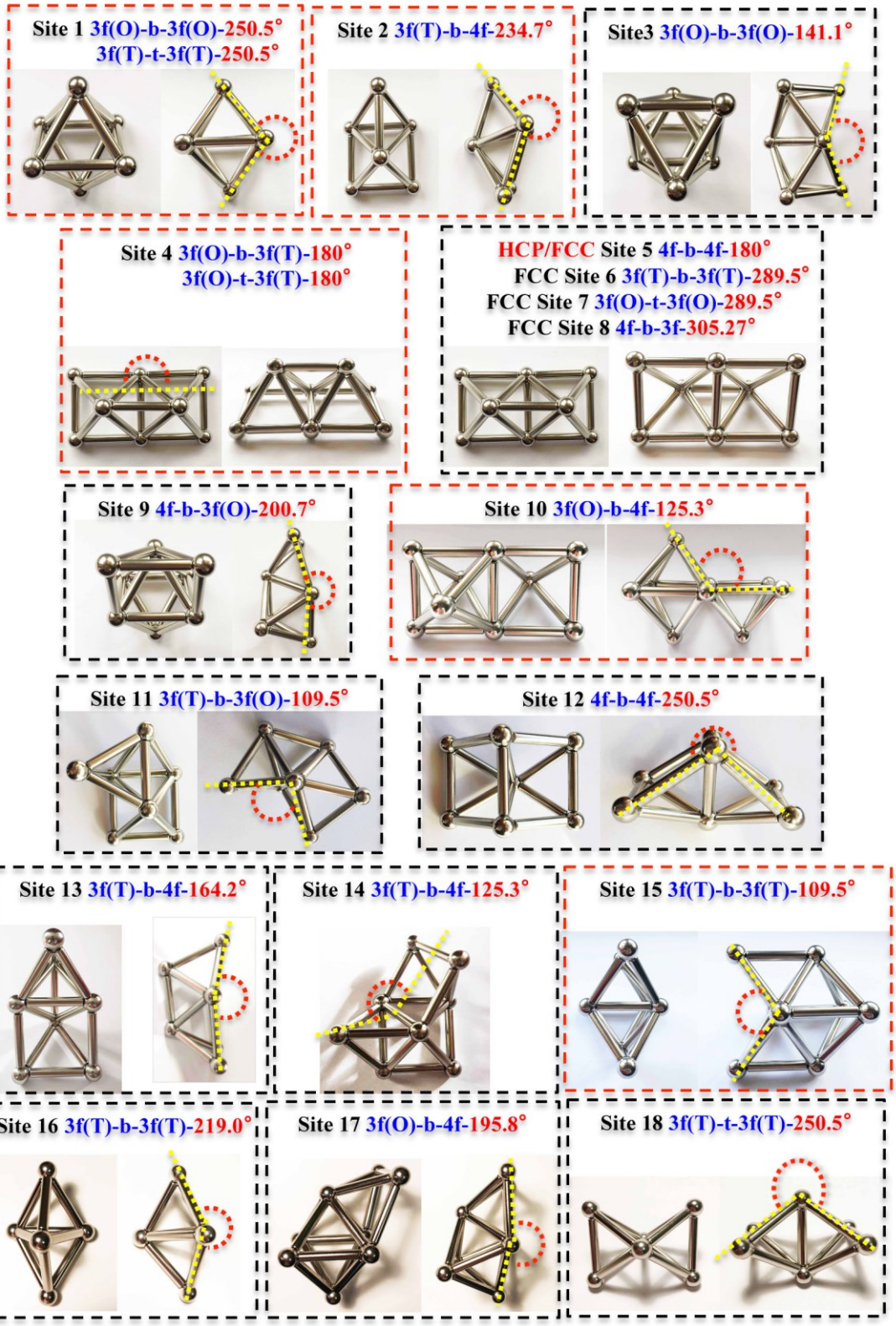
Site 1 3f(O)-b-3f(O)-250.5°
3f(T)-t-3f(T)-250.5°
Site 2 3f(T)-b-4f-234.7°
Site3 3f(O)-b-3f(O)-141.1°
Site 4 3f(O)-b-3f(T)-180°
3f(O)-t-3f(T)-180°
HCP/FCC Site 5 4f-b-4f-180°
FCC Site 6 3f(T)-b-3f(T)-289.5°
FCC Site 7 3f(O)-t-3f(O)-289.5°
FCC Site 8 4f-b-3f-305.27°
Site 9 4f-b-3f(O)-200.7°
Site 10 3f(O)-b-4f-125.3°
Site 11 3f(T)-b-3f(O)-109.5°
Site 12 4f-b-4f-250.5°
Site 13 3f(T)-b-4f-164.2°
Site 14 3f(T)-b-4f-125.3°
Site 15 3f(T)-b-3f(T)-109.5°
Site 16 3f(T)-b-3f(T)-219.0°
Site 17 3f(O)-b-4f-195.8°
Site 18 3f(T)-t-3f(T)-250.5°

Fig. 3. Various local site geometries of HCP and FCC crystals (red dash) and HCP crystals (black dashed line). The mathematical derivation of the characteristic angle is given in the appedix.

The other interesting aspect of these local catalytic sites that are identified is that in a nanocluster of just 44 atoms in HCP crystal configuration, just on one facet of the nanocluster, we can show the existence of 4 site topologies (see Fig. 4). This means that as the surface roughness increases different catalytic sites might be separated by less than a nanometer. This increases considerably the difficulty of isolating just catalytic sites of one type in metal nanoparticles. In particular on this facet of the 44 atom cluster we see the coexistence of local site 5 with the label 4f-b-4f-180°, local site 4 with the label 3f(O)-b-3f(T)-180°, local site 10 with the label 3f(O)-b-4f-125.3° and local site 1 with the label 3f(O)-b-3f(O)-250.5°. This is an amazing degree of complexity metal nanoparticles and rough surfaces can have and which deserves further investigation of such surface topologies in real catalytic systems.

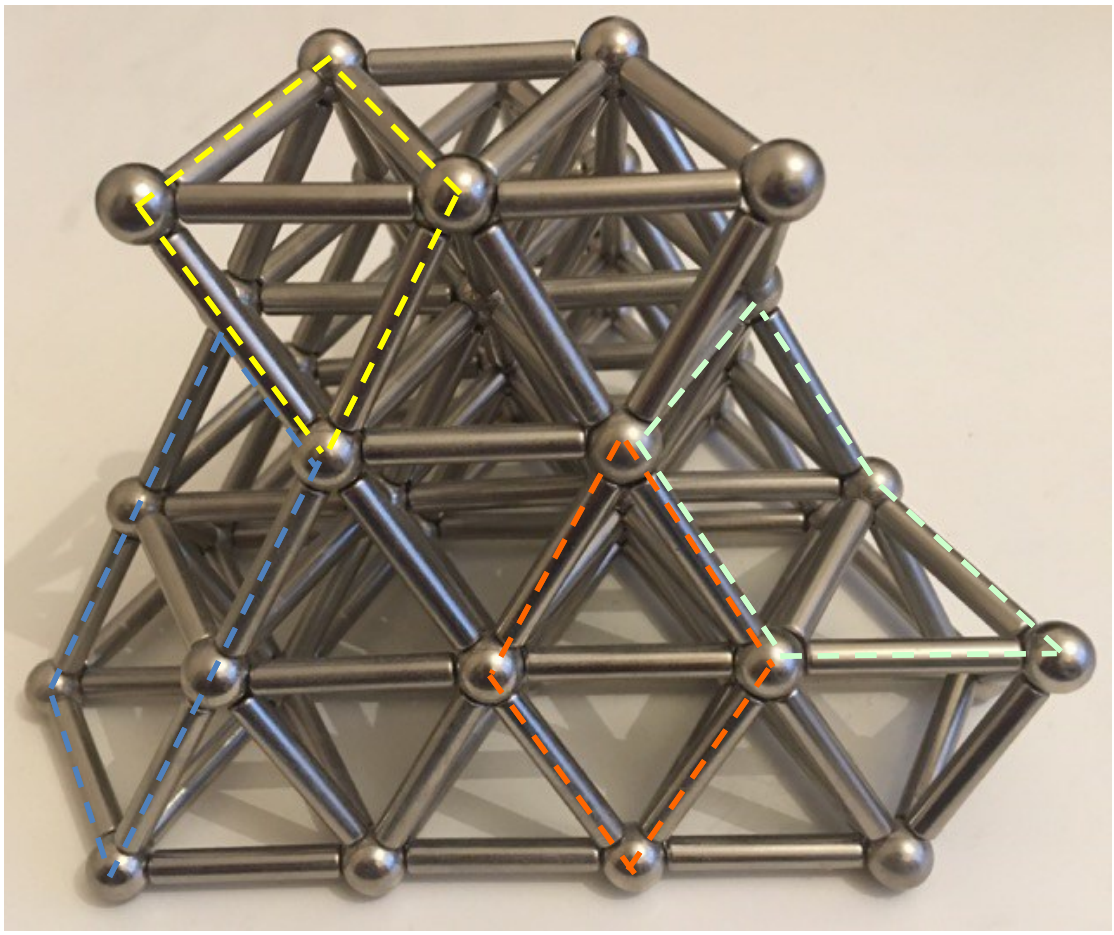

Fig. 4 Various local sites geometries embedded in a 44 atom HCP nanocluster. Local site 5 with the label 4f-b-4f-180° shown in light blue, local site 4 with the label 3f(O)-b-3f(T)-180° shown in orange, local site 10 with the label 3f(O)-b-4f-125.3° shown in light green and local site 1 with the label 3f(O)-b-3f(O)-250.5° shown in yellow.

Conclusions

We have used an analytical geometry approach to study the various local sites geometries that exist on metal NPs and surfaces of HCP and FCC crystals. The analysis points to a common notation of identifying such sites using triangular and square atom motifs that are either bridge or atop bound. Additional definition of a surface angle between such motifs can explicitly determine the site geometry. We find that the b5-site that has been previously found to be the active site for ammonia decomposition and synthesis has actually five different versions which dependent on the angle formed between the square and triangular motif. In this study we propose a convention that can be used for the identification and naming of local active site arrangements on metal NPs and surfaces present in catalysts.

Appendix

Mathematical derivation of chracteristic angle: The angles that we used for the various local sites is not based on atomic positions but based on the angle the planes form of the square pyramidal structure (θ) and the tetrahedral structure (ε). These two angles can be seen in Fig. 5 which shows that it is the angle formed between the base of the geometric shape and one of the sides of the geometric shape.

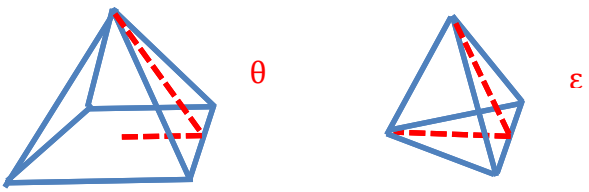

Fig. 5 Simplified schematic showing the angle betwee the planes of basic geometric shapes in HCP and FCC crystals. The angle θ = 54.735° and the angle ε = 70.528°.

These two angles if combined with the various geomtric shapes shown in Fig. 1 and Fig. 5 can give the characteristic angle of the various local sites shown in Fig. 3. Local site 1 is due to the combination of two square pyramidal shapes into one octahedron which results in a characteristic angle of $\mathbf{360°-2\theta}$ = 250.53°. Local site 2 is due to the combination of a square pyramidal and a tetrahedral geometric shape. The characteristic angle is therefore $\mathbf{360°- \theta - \varepsilon}$ = 234.7°. Local site 3 is due to the combination of a two octahedron. The characteristic angle is therefore $\mathbf{360°- 4\theta}$ = 141.06°. Local site 4 and 5 in HCP and FCC have a characteristic angle of 180°.

Local site 6 and 7 are due to the combination of two square pyramidal and a tetrahedral geometric shape. The characteristic angle is therefore $\mathbf{360°- \varepsilon}$ = 289.5°.

Local site 8 is due to the combination of two square pyramidal and a tetrahedral geometric shape. The characteristic angle is therefore $\mathbf{360°- \theta}$ = 305.2°. Local site 9 is due to the combination of an octahedron and a square pyramidal geometric shape. The characteristic angle is therefore $\mathbf{360°- \varepsilon - 2\theta}$ = 200.73°. Local site 10 is due to the combination of a two octahedron and a square pyramidal geometric shapes. The characteristic angle is therefore $\mathbf{180°- \theta}$ = 125.265°. Local site 11 is due to the combination of a square pyramidal and two tetrahedron. The characteristic angle is therefore $\mathbf{360°- 2\varepsilon - 2\theta}$ = 109.47°. Local site 12 is due to the combination of two square pyramidal geometric shapes. The characteristic angle is therefore $\mathbf{360°- 2\theta}$ = 250.53°. Local site 13 is due to the combination of a square pyramidal and two tetrahedral geometric shape. The characteristic angle is therefore $\mathbf{360°- 2\varepsilon - \theta}$ = 164.209°. Local site 14 is due to the combination of two square pyramidal and a tetrahedral geometric shape. The characteristic angle is therefore $\mathbf{360°- \varepsilon - 3\theta}$ = 125.267°. Local site 15 is due to the combination of an octahedron and two tetrahedral geometric shapes. The characteristic angle is therefore $\mathbf{360°- 2\varepsilon - 2\theta}$ = 109.47°. Local site 16 is due to the combination of two tetrahedral geometric shapes. The characteristic angle is therefore $\mathbf{360°- 2\varepsilon}$ = 219.0°. Local site 17 is due to the combination of an octahedron and a square pyramidal geometric shape. The characteristic angle is therefore $\mathbf{360°- 3\theta}$ = 195.8°. Local site 18 is due to the combination of two tetrahedron over a bridged site and the characteristic angle is $\mathbf{180° + \varepsilon}$ = 250.52°.

Conflicts of Interest

There are no conflicts of interest to declare

AUTHOR INFORMATION

Corresponding Author

*c.zeinalipour-yazdi@uel.ac.uk

REFERENCES

[1] F.R. García-García, A. Guerrero-Ruiz, I. Rodríguez-Ramos, Top. Catal. 52 (2009) 758.
[2] R. van Hardeveld, A. van Montfoort, Surf. Sci. 4 (1966) 396.
[3] C.J.H. Jacobsen, S. Dahl, P.L. Hansen, E. Törnqvist, L. Jensen, H. Topsøe, D.V. Prip, P.B. Møenshaug, I. Chorkendorff, J. Molec. Catal. A: Chem. 163 (2000) 19.
[4] S. Taylor Hugh, F. Armstrong Edward, P. Roy. Soc. A-Math. Phy. 108 (1925) 105.
[5] I. Langmuir, T. Faraday Soc. 17 (1922) 621.
[6] C.D. Zeinalipour-Yazdi, J.S.J. Hargreaves, C.R.A. Catlow, J. Phys. Chem. C 122 (2018) 6078.
[7] J. Engel, S. Francis, A. Roldan, Phys. Chem. Chem. Phys. 21 (2019) 19011.
[8] D.J. Zeyl, Plato's Timaeus (trans.), Indianapolis and Cambridge, Mass: Hackett Publishing Co. (2000).
[9] P. Ball, Nature 480 (2011) 455.
[10] F. Calle-Vallejo, J.I. Martínez, J.M. García-Lastra, P. Sautet, D. Loffreda, Angew. Chem. Int. Ed. 53 (2014) 8316.
[11] F. Calle-Vallejo, D. Loffreda, M.T.M. Koper, P. Sautet, Nat. Chem. 7 (2015) 403.
[12] F. Calle-Vallejo, J. Tymoczko, V. Colic, Q. Vu, M. Pohl, K. Morgenstern, D. Loffreda, P. Sautet, W. Schuhmann, A. Bandarenka, Science 350 (2015) 185.
[13] A. Gannouni, C. Michel, F. Delbecq, M.S. Zina, P. Sautet, Phys. Chem. Chem. Phys. 20 (2018) 25377.
[14] A. Gannouni, F. Delbecq, M. Saïd Zina, P. Sautet, J. Phys. Chem. A 121 (2017) 5500.
[15] A. Chutia, A. Thetford, M. Stamatakis, C.R.A. Catlow, Phys. Chem. Chem. Phys. 22 (2020) 3620.
[16] N. Agarwal, L. Thomas, A. Nasrallah, M.A. Sainna, S.J. Freakley, J.K. Edwards, C.R.A. Catlow, G.J. Hutchings, S.H. Taylor, D.J. Willock, Catal. Today (2020).
[17] M.D. Higham, M.G. Quesne, C.R.A. Catlow, Dalton Trans. 49 (2020) 8478.
[18] J. Engel, E. Schwartz, C.R.A. Catlow, A. Roldan, J. Mat. Chem. A 8 (2020) 15695.

[19] E. Morra, M. Signorile, E. Salvadori, E. Giamello, S. Bordiga, M. Chiesa, Angew. Chem. Inter. Edit. 58 (2019) 12398.
[20] J. Xu, Q. Wang, F. Deng, Acc. Chem. Res. 52 (2019) 2179.
[21] A.S. McLeod, Chem. Eng. Res. Des. 82 (2004) 945.
[22] C.R. Salvo, J. Keagy, J.A. Yarmoff, J. Phys. Chem. C 122 (2018) 24732.
[23] K. Gotterbarm, C. Bronnbauer, U. Bauer, C. Papp, H.-P. Steinrück, J. Phys. Chem. C 118 (2014) 25097.
[24] T. Nilsson Pingel, M. Jørgensen, A.B. Yankovich, H. Grönbeck, E. Olsson, Nature Commun. 9 (2018) 2722.
[25] Y. Takato, E. Benson Michael, S. Sen, P. Roy. Soc. A-Math. Phy. 474 (2018) 20170723.
[26] M. Melander, V. Latsa, K. Laasonen, J. Chem. Phys. 139 (2013) 164320.
[27] C.D. Zeinalipour-Yazdi, J.S.J. Hargreaves, C.R.A. Catlow, J. Phys. Chem. C 120 (2016) 21390.
[28] D.J. Henry, J. Phys. Chem. C 117 (2013) 26269.
[29] K.E.A. Batista, J.L.F. Da Silva, M.J. Piotrowski, J. Phys. Chem. C 123 (2019) 7431.
[30] I.V. Yudanov, M. Metzner, A. Genest, N. Rösch, J. Phys. Chem. C 112 (2008) 20269.
[31] H. An, S. Kwon, H. Ha, H.Y. Kim, H.M. Lee, J. Phys. Chem. C 120 (2016) 9292.
[32] P.C.P. Caldas, J.M.R. Gallo, A. Lopez-Castillo, D. Zanchet, J.M. C. Bueno, ACS Catal. 7 (2017) 2419.
[33] R. Fukuda, N. Takagi, S. Sakaki, M. Ehara, J. Phys. Chem. C 121 (2017) 300.
[34] C.D. Zeinalipour-Yazdi, D.J. Willock, L. Thomas, K. Wilson, A.F. Lee, Surf. Sci. 646 (2016) 210.